# 論文 / 著書情報
# Article / Book Information

| | |
|---|---|
| Title | Fluorinated Poly(pentylene 4,4′-bibenzoate)s with Low Isotropization Temperatures and Unique Phase Transition Behavior |
| Authors | Yoshimichi Shimomura, Masatoshi Tokita, Atsuya Kawamura, Junji Watanabe, Gen-ichi Konishi |
| Citation | Macromolecules, Vol. 56, Issue 13, pp. 5152–5161 |
| Pub. date | 2023, 6 |
| DOI | https://doi.org/10.1021/acs.macromol.3c00773 |
| Creative Commons | Information is in the article. |

Macromolecules

pubs.acs.org/Macromolecules

Article

# Fluorinated Poly(pentylene 4,4′-bibenzoate)s with Low Isotropization Temperatures and Unique Phase Transition Behavior

Yoshimichi Shimomura, Masatoshi Tokita, Atsuya Kawamura, Junji Watanabe, and Gen-ichi Konishi*

Cite This: *Macromolecules* 2023, 56, 5152−5161

Read Online

ACCESS | Metrics & More | Article Recommendations | Supporting Information

**ABSTRACT:** Semiflexible main-chain thermotropic liquid crystalline polyesters (TLCPs) are applied in functional materials like heat dissipation sheets because of their good processability and ability to form nanostructures. Poly(pentylene 4,4′-bibenzoate) (**BB-5**) is a commonly investigated biphenyl-based TLCP that forms a $SmC_A$ phase. The functional application of **BB-5** is limited by its high isotropization temperature ($T_i$). This study aims to lower the $T_i$ of **BB-5** and enhance the processability of poly(pentylene 4,4″-terphenyl dicarboxylate) (**T-5**) compounds, which contain photo/electronic functional mesogens. Six fluorinated **BB-5** (**F-BB-5**) compounds are synthesized with $T_i$ values at least 35 °C lower than that of **BB-5**. Fluorinated **T-5** (**F-T-5**) compounds show isotropic phases before thermal decompositions, unlike **T-5**. Moreover, **F-BB-5** and **F-T-5** form not only amorphous and $SmC_A$ phases but also crystalline and higher-order smectic phases, which is unexpected from low-molecular-weight liquid crystals. Mesogenic fluorination of semiflexible TLCPs results in low $T_i$ and even unique morphologies, opening up their new possibilities.

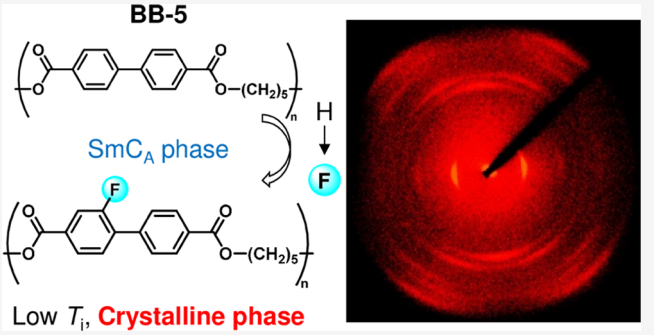




## INTRODUCTION

Aromatic main-chain thermotropic liquid crystalline polyesters (TLCPs) have been extensively investigated owing to their versatile nano-orientation and excellent functionality that are derived from their nanostructures.[1−5] They are used as (super)engineering plastics with high thermal stability, chemical resistance, and dimensional stability; low gas permeability; and excellent mechanical properties.[6−8] However, wholly aromatic TLCPs often undergo thermal degradation prior to isotropization.[9] Various aromatic polyesters have been developed to overcome this problem through copolymerization[10−15] and the use of semiflexible TLCPs,[16−18] in which flexible spacers are incorporated into the main chain.

Semiflexible TLCPs exhibit superior properties compared with those of wholly aromatic TLCPs, including melting points that are lower than degradation temperatures, low melt viscosities, and the presence of different phases, such as crystalline, smectic (Sm) A, SmC, $SmC_A$, and nematic phases.[19] One of the most extensively investigated semiflexible TLCPs is poly(pentylene 4,4′-bibenzoate) (**BB-5**), which is a biphenyl-based polyester (Chart 1). Our group reported **BB-5** for the first time in 1988 and identified its LC structure.[20,21] **BB-5** forms not only the $SmC_A$ phase in a wide temperature range (86−196 °C) but also folded-chain lamellar structures. The phase transitions of **BB-5** that are associated with the odd−even effect of alkyl spacers have also been reported.[22] Moreover, introducing methyl groups into the aliphatic spacer

**Chart 1**

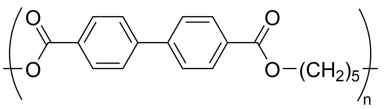

of **BB-5** produces the $SmC_A$ and SmA phase without crystallization.[23,24] Various characteristics of **BB-5**, such as its nanostructure and thermally conductivity, were enhanced because of these properties.[25] However, **BB-5** suffers from a high isotropization temperature ($T_i$: 212 °C upon heating and 196 °C upon cooling), crystallization at 86 °C upon cooling, and the absence of various morphologies.

In recent years, nanostructures of block-copolymerized semiflexible TLCPs have been studied for their potential use in nano-applications because of their ability to be aligned by external fields, such as magnetic and electric fields or shear flow.[26−29] However, new mesogenic strategies are required for the further performance improvement of these compounds, such as achieving better electrical/optical properties, lowering

**Received:** April 22, 2023
**Revised:** May 30, 2023
**Published:** June 21, 2023

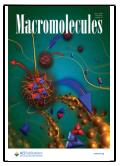

**Scheme 1. Synthesis Methods of the Poly(pentylene 4,4′-bibenzoate) (BB-5) and Poly(pentylene 4,4″-terphenyl dicarboxylate) (T-5) Derivatives**

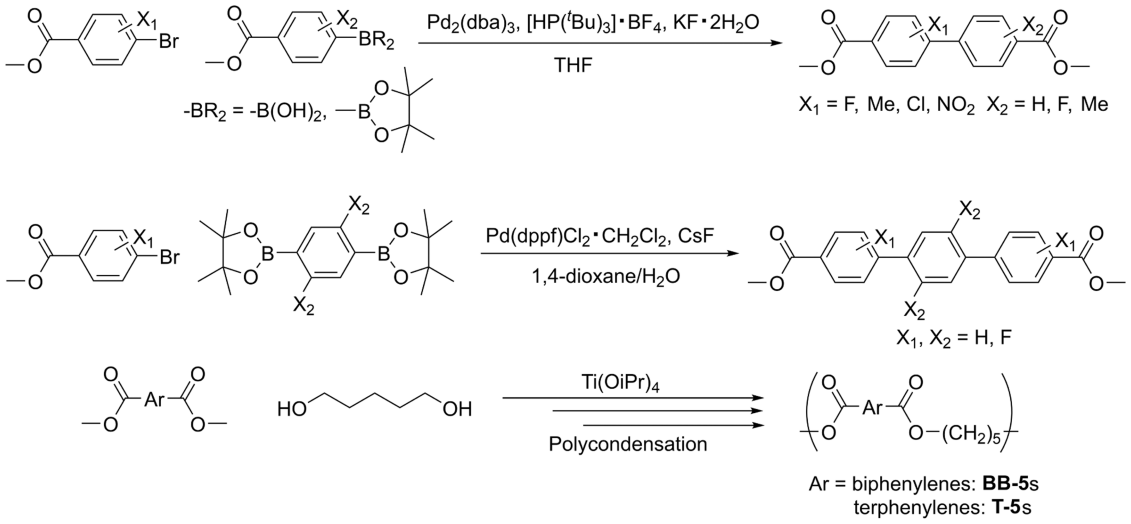


processing temperatures, and generating higher-order smectic phases.[30,31] Consequently, this study focuses on the lateral fluorine substitution of mesogenic biphenyl moieties. In low-molecular-weight liquid crystals, the lateral fluorine substitution of mesogens disrupts their molecular packing and reduces the number of intermolecular attractive forces, thus lowering the phase transition temperature and smectic phase stability.[32] For LC molecules with small-aspect-ratio mesogens, such as biphenyl-based mesogens, lateral substitution sometimes suppresses liquid crystallinity.[33] However, the effects of small substituents, such as fluorine, in the mesogenic biphenyl moieties of semiflexible TLCPs on their liquid crystalline behavior have not been examined in detail,[34] although other laterally substituted semiflexible TLCPs have been reported previously.[35,36]

In this study, we explore the effect of the lateral introduction of one or two fluorine groups on the phase transition behavior of **BB-5**. In addition, the effects of the methyl, chloro, and nitro groups were investigated. Note that nitro-substituted biphenyls sometimes form cubic phases.[37] Fluorinated **BB-5s** (**F-BB-5s**) have $T_i$ that are at least 34.3 °C lower than that of **BB-5** upon heating. **F-BB-5s** with $SmC_A$ phases do not crystallize during the cooling process, and some of them exhibit lower $T_i$ than those of conventional **BB-5s**. Lower melting and isotropic points allow not only a reduction in the processing temperature but also the use of more rigid calamitic molecules as mesogens. Based on these results, we have developed laterally fluorinated poly(pentylene 4,4″-terphenyl dicarboxylate)s **T-5s** (**F-T-5s**), which are semiflexible polyesters with terphenyl groups serving as mesogens, to obtain a smectic phase in the processable temperature range. For **T-5**, only the odd−even effect of the aliphatic spacer has been reported;[38] phase structure analysis and luminescence properties of **T-5** have not been studied in detail. Moreover, our new **F-BB-5s** and **F-T-5s** exhibit unique phase transitions, which cannot be predicted from the properties of their low-molecular-weight liquid crystals.[39,40] **F-BB-5s** contain not only the $SmC_A$ and amorphous phases but also crystalline and higher-order smectic phases, and **F-T-5s** form the $SmC_A$, crystalline, and higher-order smectic phases. These results can be derived from polymer orientations.

## EXPERIMENTAL SECTION

**General Procedure for Biphenyl Monomers.**[41] Aryl bromide (1.0 equiv), aryl boronic acid (pinacol ester) (1.1−1.2 equiv), tris(dibenzylideneacetone)dipalladium(0) ($Pd_2(dba)_3$) (0.5 mol %), tri-*tert*-butylphosphonium tetrafluoroborate (1.2 mol %), and potassium fluoride dihydride (3.3 equiv) were dissolved in tetrahydrofuran (THF). The mixture was heated at 50 °C for more than 4 h under an argon atmosphere, then filtrated through celite by diethyl ether. The filtrate was evaporated under reduced pressure. The residue was chromatographed over silica gel and recrystallized to give the target compound.

**General Procedure for Terphenyl Monomers.**[42] Aryl bromide (2.1 equiv), aryl diboronic acid pinacol ester (1.0 equiv), [1,1-Bis(diphenylphosphino)ferrocene]palladium(0) ($Pd(dppf)Cl_2·CH_2Cl_2$) (10 mol %), and cesium fluoride (6.0 equiv) were dissolved in 2:1 (v/v) 1,4-dioxane/water. The mixture was refluxed at 110 °C overnight under an argon atmosphere. Water was added, and the mixture was extracted with dichloromethane. The organic layer was washed with water three times, dried over $MgSO_4$, filtrated, and evaporated under reduced pressure. The residue was chromatographed over silica gel and recrystallized to give the target compound.

**General Procedure for Melt Polycondensation.**[20] Dimethyl ester monomer (1.0 equiv), 1,5-pentanediol (1.5 equiv), and tetraisopropyl orthothitanate ($Ti(OiPr)_4$) (catalyst amount) were set in a test tube. The test tube was replaced with nitrogen for 10 min and melt-polymerized under flowing nitrogen at 220 °C for more than 4 h. The polymer was dissolved in chloroform and precipitated into methanol to give the target polymer.

**Measurements.** $^1$H-NMR and $^{13}$C-NMR spectra were recorded on BRUKER 500 (500 MHz) and JEOL 400 (100 MHz) spectrometers, respectively, for $CDCl_3$ solution using tetramethylsilane (TMS) as an internal standard. $^1$H-NMR spectra are reported as follows: chemical shift ($\delta$ ppm), multiplicity (s = singlet, d = doublet, t = triplet, q = quartet, m = multiplet), integration, and coupling constants in units of Hz. $^{13}$C-NMR spectra are reported as chemical shifts in ppm.

High-resolution (HR) EI mass spectra were recorded on a double-focusing mass spectrometer JEOL JMS-700, measured at Tokyo Institute of Technology Open Facility Center. This center is independent of our laboratory to ensure fairness.

Size exclusion chromatography (SEC) was performed using a JASCO system (PU-4185, AS-2055, CL-NETII/ADC, CO-4060, UV-4075, RI-4035) equipped with PS gel columns (SHODEX KF-405LHQ) with $CHCl_3$ as the eluent at a flowing rate of 0.2 mL min$^{-1}$ at 40 °C after calibration with polystyrene standards.


https://doi.org/10.1021/acs.macromol.3c00773
Macromolecules 2023, 56, 5152−5161

Table 1. Thermal Properties and Number-Average Molecular Weights ($M_n$) of the Poly(pentylene 4,4′-bibenzoate)s (BB-5s) Determined Using DSC and SEC Measurements

| Structure | Entry | $T_g$ (°C) | Phase transition behavior[a] | $\Delta H_i$ (kJ mol$^{-1}$) | $Mn$ (g mol$^{-1}$) |
|---|---|---|---|---|---|
| | **BB-5 (1)** | 43 | **Cry** (173 °C) **SmC$_A$** (212 °C) **Iso** | -[b] | -[f] |
| 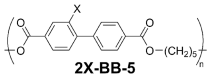 2X-BB-5 | **2F-BB-5 (2)** | - | **Cry** (131.9, 145.0 °C) **Iso** | 5.78 | 3000 |
| | **2Me-BB-5 (3)** | 44.2 | Amorphous | - | 11000 |
| | **2Cl-BB-5 (4)** | 19.9 | Amorphous | - | 2400 |
| | **2NO$_2$-BB-5 (5)** | 53.0 | Amorphous | - | 5800 |
| 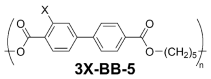 3X-BB-5 | **3F-BB-5 (6)** | 25.3 | **SmC$_A$** (177.7 °C) **Iso** | 4.10 | 14500 |
| | **3Me-BB-5 (7)** | 6.3 | No peak, but **L-Sm** | -[c] | 1200 |
| | **3Cl-BB-5 (8)** | 40.1 | Amorphous | - | 3500 |
| | **3NO$_2$-BB-5 (9)** | 50.2 | Amorphous | - | 5100 |
| 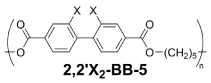 2,2′X$_2$-BB-5 | **2,2′F$_2$-BB-5 (10)** | 36.5 | Amorphous | - | 8500 |
| | **2,2′Me$_2$-BB-5 (11)** | 41.7 | Amorphous | - | 10300 |
| 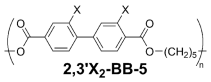 2,3′X$_2$-BB-5 | **2,3′F$_2$-BB-5 (12)** | 11.4 | No peak, but **Cry** or **H-Sm** | -[c] | 1700 |
| | **2,3′Me$_2$-BB-5 (13)** | 17.6 | Amorphous | - | 3200 |
| 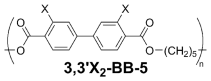 3,3′X$_2$-BB-5 | **3,3′F$_2$-BB-5 (14)** | 32.4 | **Cry** or **H-Sm** (141.1, 149.6 °C) **Iso** | 5.09[d] | 4400 |
| | **3,3′Me$_2$-BB-5 (15)** | 13.0 | Amorphous | - | 3700 |
| 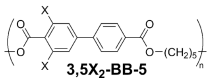 3,5X$_2$-BB-5 | **3,5F$_2$-BB-5 (16)** | 37.5 | **SmC$_A$** (87.3 °C) **Iso** | -[e] | 4900 |

[a]Phase transition behavior. [b]$\Delta H_i$ of BB-5. [c]$\Delta H_i$ of 3Me-BB-5 and 2,3′F2-BB-5. [d]$\Delta H_i$ of 3,3′F-BB-5. [e]$\Delta H_i$ of 3,5F2-BB-5. [f]Mn of BB-5.

Polarizing optical microscopy (POM) was performed using a Leica DM2500P microscopy with a METTLER TOREDO FP82HT Hot stage controlled with the METTLER TOREDO Central Processor of the FP900 System at a rate of 10 °C min$^{-1}$.

Differential scanning calorimetry (DSC) was performed using PerkinElmer DSC 8500 equipment at a scanning rate of 10 °C min$^{-1}$ under a flow of dry nitrogen. Thermo-gravimetric analysis (TGA) was performed using a Rigaku Thermo Plus EVO2 series TG-DTA 8122 at a heating rate of 20 °C min$^{-1}$ under a flow of dry nitrogen. The initial mass of the samples was 5−7 mg.

Fiber samples were prepared by spinning the isotropic melt and quenching to room temperature. Press samples were prepared by sandwiching samples between two stainless used steel sheets (95 mm × 95 mm) with 30 kN force under vacuum, annealed at an appropriate temperature for 1 h, with a Manual Hydraulic Vacuum-Heating Press (Imoto Machinery Co., Ltd., Kyoto, Japan). Wide-angle X-ray diffraction (WAXD) patterns were obtained using a Bruker D8 DISCOVER equipped with a Vantec-500 detector and Cu K$\alpha$ radiation.

## RESULTS AND DISCUSSION

We systematically designed and synthesized substituted bibenzoate monomers with fluorine atoms at the inner and/or outer lateral positions (Scheme 1) to investigate the relationship between the mesogenic structure and morphology of a substituted **BB-5**. For comparison, we also prepared bibenzoate monomers with methyl, chloro, or nitro groups at the lateral positions. Biphenyl bibenzoate monomers were prepared by Suzuki−Miyaura cross-coupling reactions from the corresponding bromobenzene and phenylboronic acid derivatives. Sixteen **BB-5** derivatives (Table 1) were synthesized by the Ti(OiPr)$_4$-catalyzed melt polycondensation of a corresponding monomer and 1,5-pentanediol (Scheme 1). Moreover, we developed fluorine-substituted terphenyl-based polyester **T-5s** to produce large-aspect-ratio mesogens with optical, luminescent, and electrical properties derived from the extended-conjugation length. All dimethyl ester monomers were measured by $^1$H- and $^{13}$C- NMR except for **3,2′,5′,3″F$_4$-monomer** that could not be measured by $^{13}$C-NMR due to its poor solubility in deuterated chloroform. $^1$H-NMR and SEC measurements were performed on the chloroform-soluble polymers. DSC measurements were performed on the **BB-5** derivatives at a rate of 10 °C min$^{-1}$ (Figures 1a and S1−S15). POM observations were performed on all polymers except **BB-5** at a rate of 10 °C min$^{-1}$ (Figures 1c and S16−S25). WAXD measurements were performed on polymers that showed phase transition behaviors in the POM measurements (Figures 1d, 2a, and Figures S26−37). TGA measurements were performed on four of the **T-5** derivatives at a rate of 20 °C min$^{-1}$ (Figures S38−41).

**Laterally Substituted BB-5s.** In previous studies, we demonstrated the specificity of **BB-5** (**1**) compared to **BB-6**.[21] **BB-6** has a SmA phase and approximately parallel mesogens and alkyl chains. This characteristic is similar to the low-molar-mass SmA phase.[43] In contrast, **1** forms the SmC$_A$ phase by tilting mesogens in the polymer chains by approximately 25° with respect to the chain axis. The mesogens adjacent along the chain tilt in opposite directions. This zigzag conformation is due to the effect of connecting mesogens via most extended spacers, which do not occur in the low-molar-mass SmC phase.



https://doi.org/10.1021/acs.macromol.3c00773
Macromolecules 2023, 56, 5152−5161

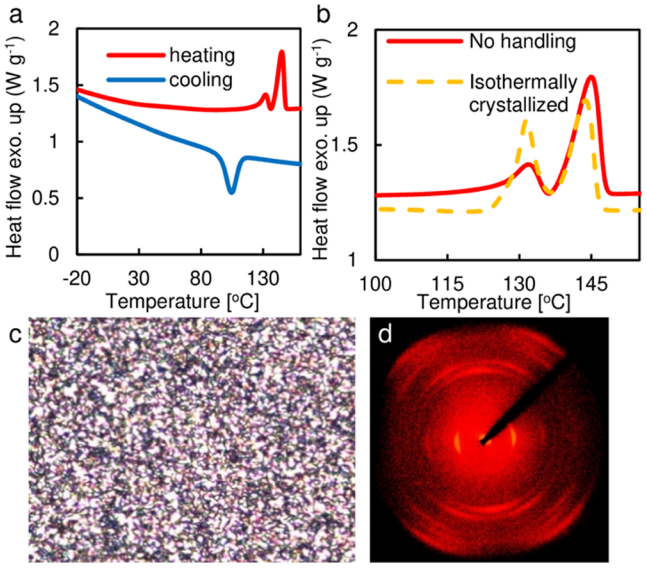


**Figure 1.** DSC thermograms of (a) **2** and (b) its unhandled and isothermally crystallized derivates measured at a rate of 10 °C min$^{-1}$. (c) POM image of **2** being cooled at 95 °C. (d) WAXD pattern for the fiber sample of **2** annealed at 135 °C for 1 h. The fiber axis lies in the horizontal direction.

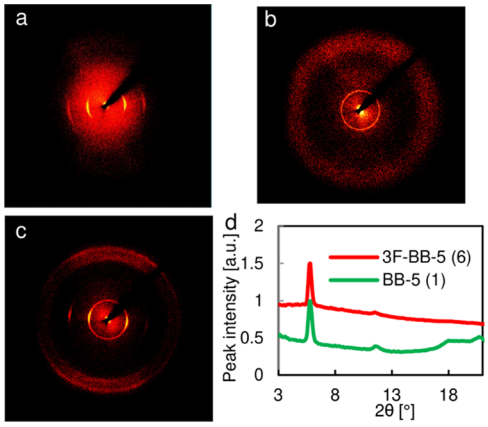


**Figure 2.** WAXD patterns for the (a) fiber sample of **6** annealed at 60 °C for 1 h, (b) bulk sample of **6** measured at 150 °C, and (c) fiber sample of **1** annealed at 190 °C for 1 h. The fiber axis lies in the horizontal direction. (d) WAXD intensity profiles measured for **1** and **6**. The circles show secondary reflections.

Alkylene 4,4′-bibenzoates do not have liquid crystallinity,[44] while **1** forms a liquid crystalline phase because of the extension of the aspect ratio to the ester group. In the condensed phase, the mesogenic ester groups of **BB-5** become coplanar because of the immobilization of the polymer and the aspect ratio increases, resulting in the development of liquid crystalline properties. The phase transition behavior of **1** in ref 22 is as follows: during the heating process, **1** melts at 173 °C to form $SmC_A$, which transforms into the isotropic liquid at 212 °C. In this study, **F-BB-5s** have $T_i$ values that are at least 34 °C lower than that of **BB-5**. Furthermore, the morphologies, such as the amorphous, $SmC_A$, crystalline, and higher-order smectic phases, depend on the position and number of fluorine atoms. In contrast, almost all of the other group (methyl, chloro, and nitro)-substituted **BB-5s** are amorphous. The glass-transition temperatures ($T_g$), phase transition behaviors, transition enthalpies (to isotropic) ($\Delta H_i$), and number-average molecular weights ($M_n$) of each **BB-5** derivative during heating are listed in Table 1, and the *d*-spacings are listed in Table S1. The liquid crystallinity of polyesters is independent of molecular weight, as previously reported.[45] Therefore, the relationship between the number-average molecular weight ($M_n$) and liquid crystallinity has not been considered.

The $\Delta H_i$ of **1** was reported in ref 22 (5.31 kJ mol$^{-1}$) and ref 20 (3.85 kJ mol$^{-1}$) during cooling. We resynthesized and evaluated **1** to compare its $\Delta H_i$ to that of the substituted **BB-5s** under the same measurement conditions as this study (Figure S1). However, the results differ from those in the previous study.[22] Compound **1** has phase transition peaks at 170.1 and 198.2 °C during the heating process, which overlapped. Although we could not compare the $\Delta H_i$ of the substituted **BB-5s** with that of **1**, the $\Delta H_i$ data are shown because it is a critical parameter in the liquid crystalline molecules.

**2X-BB-5.** **2F-BB-5** (**2**) shows two phase transition peaks at 131.9 and 145.0 °C upon heating with $\Delta H$ values of 1.71 and 5.78 kJ mol$^{-1}$, respectively (Figure 1a). The WAXD pattern shows some peaks in the wide-angle region (Figure 1d), and the *d*-spacing is 14.5 Å, which is 0.9 Å shorter than that of **1**. Based on the many diffraction peaks in the WAXD pattern and the short *d*-spacing, it is concluded that **2** is a crystalline polymer. For a more detailed discussion of the phase transition behavior, we also considered the DSC measurement of an isothermally crystallized sample of **2** that was annealed at 115 °C for 22 h at a heating rate of 10 °C min$^{-1}$ (Figure 1b). The higher-temperature peaks in the melting thermograms of the untreated and isothermally crystallized samples of **2** do not significantly differ. However, the lower-temperature peak of the isothermally crystallized sample is larger and sharper than that of the untreated sample. Moreover, the two phase transition temperatures are almost the same. These results indicate that **2** has two crystalline structures with different crystallization rates. However, the WAXD patterns of the fiber sample of **2** at 65 °C (Figure S26) are similar to those at 135 °C. Therefore, we could only observe a crystal structure with a higher melting peak. **2Me-BB-5** (**3**), **2Cl-BB-5** (**4**), and **2NO$_2$-BB-5** (**5**) exhibit no phase transition peaks in the DSC measurements. Moreover, **3** and **4** show no birefringence in the POM observations. Thus, **3** and **4** are amorphous. In contrast, **5** appears to form a phase, as observed by POM (Figure S16). However, most of the field of view is dark, and the WAXD pattern of the fiber sample includes only a circular halo in the wide-angle region (Figure S27), indicating that **5** is also amorphous.

**3X-BB-5.** **3F-BB-5** (**6**) shows a phase transition at 177.7 °C with a $\Delta H_i$ of 4.10 kJ mol$^{-1}$ upon heating. The WAXD pattern for the fiber sample of **6** shows peaks at $2\theta$ = 5.8 and 11.5°. In addition, no halo is observed in the wide-angle region (Figure 2a), whereas for the bulk sample of **6**, a halo is observed (Figure 2b). These primary and secondary reflections are associated with a layered structure with a *d*-spacing of 15.2 Å. This *d*-spacing coincides with that measured for **1** (15.3 Å) (Figure 2c,d). Considering the odd−even effect of the alkyl spacer, it is reasonable to assume that **6** exhibits the $SmC_A$ phase, although no halo is present in the wide-angle region in the fiber sample. The lack of halo observations is due to the lack of sample thickness. The $T_i$ value of **6** is 34.3 °C lower than that of **1** and only demonstrated a $SmC_A$ phase. The absence of crystallization is advantageous for material


https://doi.org/10.1021/acs.macromol.3c00773
Macromolecules 2023, 56, 5152−5161

processing. The $\Delta H_i$ of **6** is 1.6 kJ mol$^{-1}$ smaller than that of **2**. In general, the $\Delta H_i$ of the transition from the lower-order smectic to the isotropic phase is smaller than that of the crystalline/higher-order smectic to the isotropic phase, which supports that **2** is a crystalline polymer. **3Me-BB-5** (**7**) also shows some phases, as revealed by the DSC measurements (Figure S6) and POM observations (Figure S18). The oriented sample of **7** could not be prepared because of its low $T_g$. Thus, we performed a WAXD measurement for an unoriented sample of **7** sandwiched between thin glass films. The WAXD pattern demonstrates a primary reflection and a halo in the wide-angle region with a *d*-spacing of 15.0 Å (Figure S28). Therefore, **7** forms the $SmC_A$ phase owing to its *d*-spacing. **3Cl-BB-5** (**8**) and **3NO$_2$-BB-5** (**9**) show no phase transition behaviors in either the DSC measurements or POM observations and are determined to be amorphous.

**2,2′X$_2$-BB-5.** Neither **2,2′F$_2$-BB-5** (**10**) nor **2,2′Me$_2$-BB-5** (**11**) show phase transition peaks or formations. Compounds **10** and **11** are amorphous.

**2,3′X$_2$-BB-5.** Although **2,3′F$_2$-BB-5** (**12**) shows no phase transition peaks on the DSC chart (Figure S11), the POM observation reveals that **12** forms some phase when it is left at room temperature (Figure S20). The WAXD pattern shows many peaks at $2\theta$ = 1.8, 5.9, 14.7, 16.2, and 20.3° (Figures S30 and S31, Table S2), and the *d*-spacing of **12** was 15.0 Å, 0.4 Å shorter than that of **1**. Therefore, **12** exhibits a crystalline or higher-order smectic phase. In contrast, **2,3′Me$_2$-BB-5** (**13**) is amorphous because its phase transition peak and birefringence are not observed.

**3,3′X$_2$-BB-5.** **3,3′F$_2$-BB-5** (**14**) demonstrates a double-melting behavior (Figure S13a). The WAXD pattern shows three peaks that are different from those of SmA, SmC, and $SmC_A$ (Figures S32 and S33). To analyze the double-melting behavior, we performed the same measurements on **14** as on **2** (Figure S13b). The isothermally crystallized sample annealed at 125 °C does not show a lower melting peak, indicating that the lower melting peak is derived from a thermally unstable organization with poor integrity upon rapid cooling. This phenomenon is observed in several (semi)crystalline polymers.[46] Moreover, the total $\Delta H_i$ of **14** is 0.99 kJ mol$^{-1}$ larger than that of **6**, reinforcing the validity that **14** forms a three-dimensional ordered structure. Therefore, based on the similarity to **12**, it is assumed that **14** forms a crystalline or higher-order smectic phase. **3,3′Me$_2$-BB-5** (**15**) also has a phase transition peak at 32.7 °C upon heating but the POM observation shows a dark region. Therefore, **15** is amorphous.

**3,5X$_2$-BB-5.** **3,5F$_2$-BB-5** (**16**) exhibits both endothermic and exothermic peaks upon heating (Figure S15). The $T_i$ upon heating is 87.3 °C, which is 124.7 °C lower than that of **1**. The WAXD pattern is the same as that of **6**, with a *d*-spacing of 15.5 Å (Figure S34). Compound **16** has the $SmC_A$ phase and the lowest $T_i$ among **F-BB-5s**, with a $T_g$ above room temperature, and does not crystallize.

The $T_i$ values of **F-BB-5s** are lower than that of **1**. Compounds **6**, **10**, and **16** do not exhibit crystalline phases, unlike **1**. Moreover, **10** does not exhibit a smectic phase, suggesting that these polyesters are affected by the steric hindrance of fluorine. In contrast, **2** is a crystalline polymer, and both **12** and **14** forms crystalline or higher-order smectic phases. In biphenyl-type low-molecular-weight liquid crystals, the introduction of fluorine into lateral positions decreases the melting and isotropic points, which sometimes leads to a reduction in the liquid crystallinity. In other words, the molecular orientation is reduced and the crystal structure formation is more complicated. However, in **BB-5**, the formation of higher-order structures predominates depending on the positions of the fluorine substitutions. Polymer immobilization plays a significant role in this process and provides unpredictable results for small liquid crystalline molecules.

Of the methyl-, chloro-, and nitro-substituted derivates of **BB-5**, only **7** shows phase formation. However, the average molecular weight of **7** is 1200 (Table 1), which is considerably lower than that of the other polymers and may influence the phase formation. The aspect ratio of a biphenyl mesogen is insufficient when the substituents are larger than the methyl group, and most polymers are amorphous.

In general, the crystalline and higher-order smectic structures of organic compounds are highly dependent on thermodynamic factors. In addition, a detailed analysis of these polymers is complicated. Press samples of **12** and **14** prepared in this study are not uniaxially oriented, and their WAXD patterns show circular reflection peaks. Moreover, polymers rarely form tetragonal or hexagonal crystals, and the crystal lattice of only a few polymers can be determined by their *d*-spacings despite being uniaxially oriented. Therefore, a detailed analysis of the crystalline or higher-order smectic structures of **2**, **12**, and **14** is difficult. In this study, we do not focus on a detailed consideration of their structures and instead investigate the development of a new method for controlling the morphology of **BB-5**.

**F-T-5s.** The phase transition behavior and degradation temperatures at a 10% weight loss ($T_{10}$) of **T-5** (**17**) and **F-T-5s** are shown in Table 2. The POM images of these compounds are shown in Figures S23−S25 and their WAXD patterns are shown in Figures 3 and S35−S37. In the POM observations, **17** thermally decomposes before the isotropization, whereas all of **F-T-5s** exhibit $T_i$ values during the heating process. All **T-5s** exhibit similar $T_{10}$ values at approximately 404 °C, which was higher than the $T_i$ values of **F-T-5s**. Thus, lateral fluorine substituents in the mesogens allow the

**Table 2. Thermal Properties of T-5s**

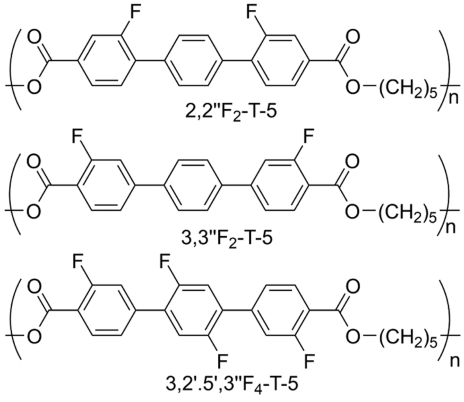


| entry | phase transition behavior[a] | $T_{10}$ (°C)[b] |
|---|---|---|
| **T-5** (**17**) | **Cry** or **Sm**, decomposed | 407.3 |
| **2,2″F$_2$-T-5** (**18**) | **Cry** or **H-Sm** (290.1 °C) **Iso** | 404.5 |
| **2,3″F$_2$-T-5** (**19**) | **SmC$_A$** (311.3 °C) **Iso** | 407.4 |
| **3,2′,5′,3″F$_4$-T-5** (**20**) | **Cry** (240.4 °C) **Iso** | 398.2 |

[a]Recorded from POM observation at a heating rate of 10 °C min$^{-1}$. [b]Recorded from TGA measurements at a heating rate of 20 °C min$^{-1}$.


https://doi.org/10.1021/acs.macromol.3c00773
Macromolecules 2023, 56, 5152−5161

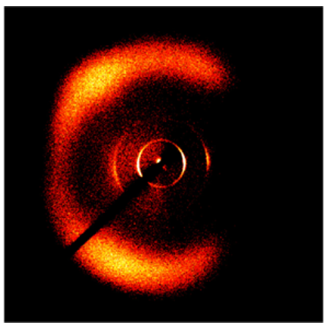

**Figure 3.** WAXD pattern for the press sample of **3,3″F$_2$-T-5** (**19**) annealed at 200 °C for 1 h, as viewed from the edge. (The right side of the WAXD pattern is dark owing to the malfunction of the measurement equipment).

processing of semiflexible TLCPs whose mesogens are electrically or optically functional molecules, such as terphenyl.

The WAXD pattern of **3,3″F$_2$-T-5** (**19**) shows a typical SmC$_A$ pattern with *d*-spacing of 18.2 Å (Figures 3 and S37). Meanwhile, **2,2″F$_2$-T-5** (**18**) shows a pattern different from those of the SmA, SmC, and SmC$_A$ phases (Figures S35 and S36). The *d*-spacing of **18** is 19.7 Å, which is 1.5 Å longer than that of **19**. However, **18** can have a crystalline or higher-order smectic phase for the following reasons: there are more than three peaks present in the WAXD pattern of **18**, its solubility in chloroform is relatively poor compared with that of **19**, or the sample of **18** is tough. **3,2′,5′,3″F$_4$-T-5** (**20**) is nearly insoluble in chloroform and the sample is also tough. Furthermore, **20** shows a phase formation that resembled needle growth, as observed in POM at 230 °C during cooling (Figure S25). These results indicate that **20** forms a crystalline phase.

**Conformational Study of Fluorinated Mesogenic Moieties.** The behavior of bibenzoate in the monomer and polymer was theoretically analyzed. We calculated the rotational energy of an ester group and the molecular orbital of bibenzoate with a dihedral angle ($\varphi$) between the ester and biphenyl groups (Figure 4a) of 0 and 90° using density functional theory at the $\omega$B97XD/6-311G(d, p) level of theory.[47] The rotational barrier of $\varphi$ = 60° is approximately 20 kJ mol$^{-1}$ and that of $\varphi$ = 90° is approximately 30 kJ mol$^{-1}$. However, since dialkyl bibenzoates are relatively large, they

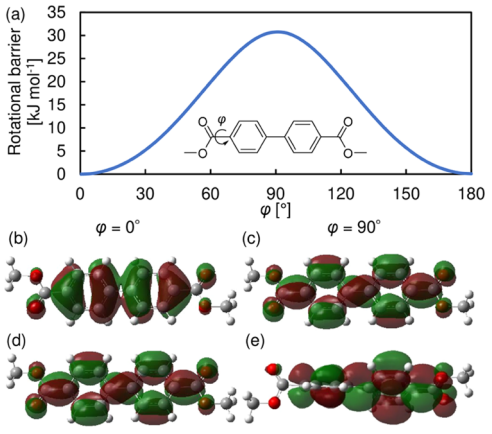


**Figure 4.** (a) Rotational barrier of bibenzoate. (b) HOMO and (c) LUMO of bibenzoate at $\varphi$ = 0°. (d) HOMO and (e) LUMO of bibenzoate at $\varphi$ = 90°.

have $T_i$ values higher than 40 °C.[44] Thus, the ester group of bibenzoate can rotate in an isotropic phase. In addition, in $\varphi$ = 0°, the $\pi$-electron cloud extends from the biphenyl group to the ester group (Figure 4b,c), whereas in $\varphi$ = 90°, this $\pi$-electron cloud extension disappears (Figure 4d,e). These results suggest that, in a monomer, the $\pi$-conjugation of bibenzoate does not extend stably to ester groups because of their rotation or the sufficient existence of $\varphi$ = nonzero conformation, and the mesogen is only biphenyl. However, owing to polymerization, the existence probability of the parallel state between ester and biphenyl groups is increased, or ester groups are immobilized in the parallel state due to the strengthened viscosity in condensed phases. Therefore, the ester groups form pseudo-conjugates to which the mesogens are extended. Pseudo-conjugation of mesogens in the liquid crystal and crystalline states of main-chain liquid crystal polymers have been reported for several mesogens with ester and urethane linkages.[48,49] However, the electronic state and structure of mesogens in the liquid crystalline state have not been discussed in detail. The bibenzoate monomer is not liquid crystalline,[44] only polymer **BB-5** is. The present calculations indicate that the pseudo-conjugation effect plays an important role in the liquid crystallinity of **BB-5**. Thus, it can be reasonably explained that the liquid crystalline nature of polybibenzoate appears due to polymeric effects.

For a more detailed discussion, we calculated the structural optimizations and rotational barriers of fluorinated biphenyls using the above theory, where (s) and (o) denote the same and opposite sides, respectively (Figures 5, S42, and S43). In liquid crystalline phases, mesogens are not completely confined and exhibit molecular motions, such as axis rotations. However, the molecular motions of the mesogenic ester groups are small in the crystalline and smectic phases of **BB-5**. Therefore, we hypothesized that the structures of the ester groups could be fixed and focused only on the biphenyl units.

The dihedral angles ($\psi$) of 3F-biphenyl and 3,5F$_2$-biphenyl are nearly identical to those of biphenyl, indicating that **6** and **16** exhibit SmC$_A$ like **1**. 3,3′F$_2$(s)/(o)-biphenyl also exhibit a similar $\psi$ to that of biphenyl. However, **14** forms a crystalline or higher-order smectic phase. Using the above theory, we also calculated the HOMO and dipole moments of bibenzoate (**A**) and 3,3′F$_2$-bibenzoates (**B**−**D**) in each conformation in the ground state (Table 3 and Figure S44).

The HOMOs of **B**−**D** are not significantly different from that of **A**, except for the electron clouds that extend to fluorine. The dipole moments differ depending on the conformation. **A**, **C**, and **D** only have the *z*-direction component, whereas **B** also has an all-direction component, with the y-direction component being the largest. The dipole moment values of **B** and **C** are one-and-a-half times larger than that of **A**, while that of **D** is one-third smaller than that of **A**. **D** has the lowest total energy among **B**, **C**, and **D**, and the energy difference between **B** and **D** is 3.65 kJ mol$^{-1}$ and that between **C** and **D** is 7.06 kJ mol$^{-1}$ (Table S4). These energy differences are so small that 3,3′F$_2$-bibenzoate can form all of the conformations of **B**, **C**, and **D**, even though the optimum structure of 3,3′F$_2$-bibenzoate is **D**. The large dipole moment of 3,3′F$_2$-bibenzoate, depending on the conformation, enhances the dipole−dipole interaction between the mesogens and would allow the formation of a higher-order structure. The $\psi$ values of 2F-biphenyl and 2,3′F$_2$(s)/(o)-biphenyl are approximately 5° larger than that of biphenyl. The combination of the fact that the electronic interactions between the mesogens become


https://doi.org/10.1021/acs.macromol.3c00773
Macromolecules 2023, 56, 5152−5161

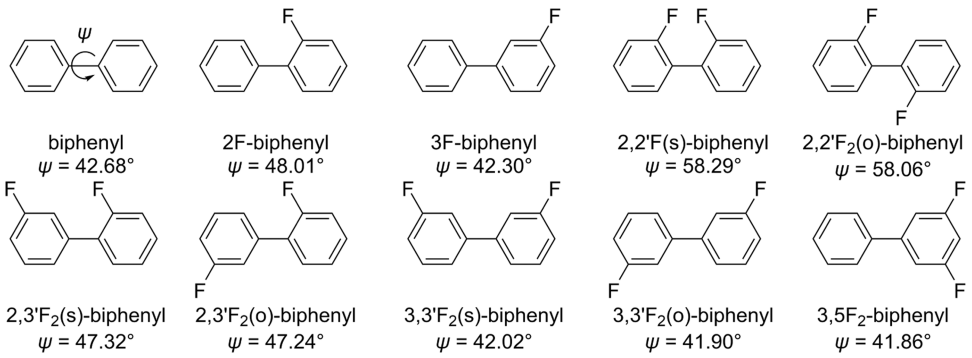


**Figure 5.** Chemical structures and calculated dihedral angles ($\psi$) of biphenyl and fluorinated biphenyls.

**Table 3. Calculated Dipole Moments of Bibenzoate and 3,3′$F_2$-Bibenzoate in Each Conformation**[a]

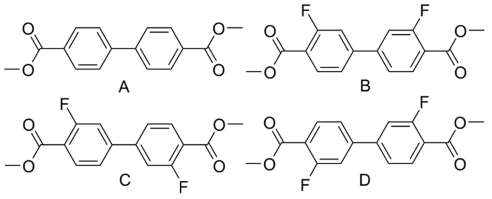


| entry | $x$ [D] | $y$ [D] | $z$ [D] | total [D] |
|---|---|---|---|---|
| A | 0 | 0 | 1.22 | 1.22 |
| B | −0.21 | −2.11 | −1.08 | 2.38 |
| C | 0 | 0 | 1.90 | 1.90 |
| D | 0 | 0 | −0.37 | 0.37 |

[a] $x$: short-axis direction; $y$: long-axis direction; $z$: perpendicular direction of $\pi$-plane.

not too small and the larger rotation barriers of $\psi$ = 0 and 180° than that of biphenyl (Table S3) may allow **2** and **12** to form crystalline and higher-order smectic phases. The $\psi$ of 2,2′$F_2$(o)-biphenyl is 50.86° and that of 2,2′$F_2$(s)-biphenyl is 58.29°. The large mesogenic twist results in very few electrical interactions. Consequently, **10** becomes an amorphous polymer. We also calculated the optimized conformation of **F-T-5**s; the results have the same trend as to those of **F-BB-5**s (Figure S45).

**Summary for Morphologies.** This study is summarized as follows (Figure 6). In condensed phases, such as liquid crystals and films, ester groups form pseudo-conjugates. As a result, the aspect ratio of the mesogen increases from biphenyl (monomer) to bibenzoate (polymer). Regarding the aspect ratio of **BB-5**, one or two lateral fluorine substitutions in the mesogen do not affect its orientation ability of **BB-5**. **F-BB-5s** possess lower $T_i$ contents than **BB-5**. Lowering the $T_i$ improves the processability of the polymer and the construction of nanostructures using a block polymer. Moreover, **F-T-5s** with a 4,4″-terphenyl diester as the mesogen exhibit $T_i$ values below their $T_{10}$, which is different from that of **T-5**. This result allows electrical and optical functional molecules to be treated as mesogens in semiflexible TLCPs.

Polymers tend to show crystalline or higher-order smectic phases (**2**, **12**) when fluorine is introduced into the mesogen on the inner side, and polymers are subject to smectic properties similar to **BB-5** (**6**, **16**) when introduced on the outer side. This trend has also been observed for **F-T-5s** (**18**, **19**, **20**). However, when the planarity of the mesogen is severely disrupted, the polymers become amorphous, such as

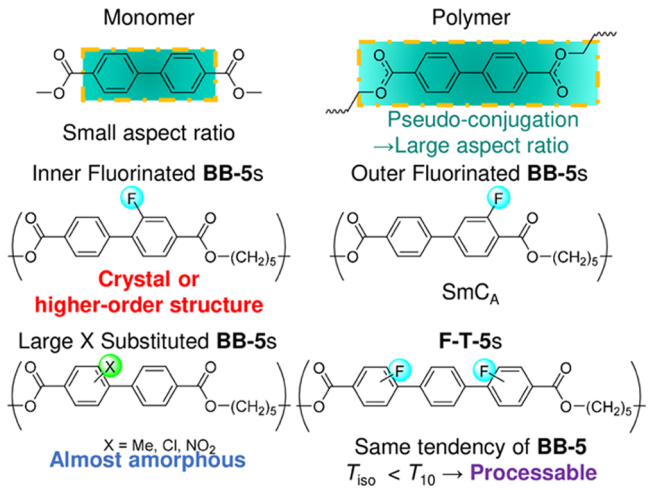


**Figure 6.** Summary of the properties of substituted poly(pentylene 4,4′-bibenzoate) (**BB-5**) and fleorinated poly(pentylene 4,4″-terphenyl dicarboxylate) (**T-5**).

**10** with fluorine substitutions at the 2- and 2′-positions of the biphenyl mesogen. However, if the substitution sizes are larger than the methyl group, nearly all of the substituted **BB-5s** are amorphous because the substitution sizes are too large relative to the mesogen of **BB-5**. Some **F-BB-5s** form structures different from $SmC_A$. However, we cannot provide a sufficient argument for this phenomenon. Moreover, the construction of a different phase structure expands the variety of polycrystals that can be formed from liquid crystal phases and contributes to the improvement of devices with higher-order structures, such as organic liquid crystal semiconductors.[30]

## CONCLUSIONS

We decreased the $T_i$ of polybibenzoate **BB-5** by at least 34.3 °C by introducing fluorine groups at the appropriate lateral positions of biphenyl mesogens. The introduction of lateral fluorine substituents usually decreases the melting and isotropic points and smectic phase stabilities of low-molecular-weight liquid crystals. The same behavior is observed for **F-BB-5s**. In particular, **3,5$F_2$-BB-5** exhibits $T_i$ at 87.3 °C and contained only the $SmC_A$ phase. These properties overcome the major limitations of conventional **BB-5** derivatives. We adjusted this strategy for terphenyl mesogen-based liquid crystalline **T-5s** by decreasing the $T_i$ of **F-BB-5s**. **F-T-5s** exhibit $T_i$ below their thermal degradation temperatures. Lateral fluorine substituents in mesogens enable the processing of **T-5** and demonstrate the advantages of lateral


https://doi.org/10.1021/acs.macromol.3c00773
Macromolecules 2023, 56, 5152−5161

fluorination in semiflexible TLCPs. These results may facilitate the practical application of main-chain TLCPs with electrically and optically functional molecules serving as mesogens. They can also be used to overcome the disadvantages of the nanostructures formed by liquid crystalline block polymers and increase the choice of mesogens. In contrast to the $T_i$, we observe unexpected morphologies for **F-BB-5s** and **F-T-5s**. **3F-BB-5**, **2,3′F$_2$-BB-5**, **3,3′F$_2$-BB-5**, **2,2″F$_2$-T-5** and **3,2′,5′,3″F$_4$-T-5** exhibit only crystalline or higher-order smectic phases. The introduction of fluorine into the inner lateral positions of the mesogens promotes the formation of crystalline or higher-order smectic phases. This feature differs from that of low-molecular-weight liquid crystals; however, the reason for this phenomenon remains unclear. It is hypothesized that the steric hindrance of fluorine causes small misalignments (distortions) in the mesogen structure compared with that of **BB-5**, and the spacers are adjusted to resolve this issue, resulting in a dense state. The unique behavior observed in this study is due to the immobilizing effect of the polymer.

In summary, the underlying mechanism of the formation of unique morphologies is elucidated, introduction of fluorine at appropriate positions is investigated, and new functional groups for TLCP improvement are developed. Lowering $T_i$ and forming even crystalline or higher-order smectic phases have great advantages for improving functional materials/devices, such as heat sinks,[50] liquid crystalline organic semiconductors,[30] high-birefringence materials,[51,52] and high-strength materials.[53] Thus, Liquid crystalline polyesters based on fluorinated oligophenylene mesogens have potential applications in a wide range of materials and devices.

## ■ ASSOCIATED CONTENT

### Supporting Information

The Supporting Information is available free of charge at https://pubs.acs.org/doi/10.1021/acs.macromol.3c00773.

Synthetic procedures in detail; $^1$H- and $^{13}$C-NMR spectra; HRMS spectra; SEC curves; DSC thermograms; POM images; WAXD patterns; TG curves; and computational results (PDF)

## ■ AUTHOR INFORMATION


### Corresponding Author

**Gen-ichi Konishi** − *Department of Chemical Science and Engineering and Department of Polymer Chemistry, Tokyo Institute of Technology, Tokyo 152-8552, Japan;* orcid.org/0000-0002-6322-0364; Email: konishi.g.aa@m.titech.ac.jp

### Authors

**Yoshimichi Shimomura** − *Department of Chemical Science and Engineering and Department of Polymer Chemistry, Tokyo Institute of Technology, Tokyo 152-8552, Japan*

**Masatoshi Tokita** − *Department of Chemical Science and Engineering and Department of Polymer Chemistry, Tokyo Institute of Technology, Tokyo 152-8552, Japan;* orcid.org/0000-0002-4534-7337

**Atsuya Kawamura** − *Department of Chemical Science and Engineering and Department of Polymer Chemistry, Tokyo Institute of Technology, Tokyo 152-8552, Japan*

**Junji Watanabe** − *Department of Chemical Science and Engineering and Department of Polymer Chemistry, Tokyo Institute of Technology, Tokyo 152-8552, Japan*

Complete contact information is available at: https://pubs.acs.org/10.1021/acs.macromol.3c00773


### Notes

The authors declare no competing financial interest.

## ■ ACKNOWLEDGMENTS

The authors thank Kosuke Yokota and Alto Hori for support for the synthesis of BB-5s. They also thank Mr. Masato Koizumi (Materials Analysis Division, Tokyo Institute of Technology) for the HRMS measurements. This research was supported in part by MEXT/JSPS KAKENHI grant 23H05145 (GK) and by the Toshiaki Ogasawara Memorial Foundation (GK).

## ■ REFERENCES


(1) Jackson, W. J., Jr Liquid crystal polymers. XI. Liquid crystal aromatic polyesters: Early history and future trends. *Mol. Cryst. Liq. Cryst.* **1989**, *169*, 23−49.

(2) Jin, J.-I.; Kang, C. S. Thermotropic main chain polyesters. *Prog. Polym. Sci.* **1997**, *22*, 937−973.

(3) Ji, Y.; Bai, Y.; Liu, X.; Jia, K. Progress of liquid crystal polyester (LCP) for 5G application. *Adv. Ind. Eng. Polym. Res.* **2020**, *3*, 160−174.

(4) Guan, Q.; Picken, S. J.; Sheiko, S. S.; Dingemans, T. J. High-temperature shape memory behavior of novel all-aromaic $(AB)_n$-multiblock copoly(ester imide)s. *Macromolecules* **2017**, *50*, 3903−3910.

(5) Watanabe, Y.; Kato, R.; Fukushima, K.; Kato, T. Degradable and nanosegregated elastomers with multiblock sequences of biobased aromatic mesogens and biofunctional aliphatic oligocarbonates. *Macromolecules* **2022**, *55*, 10285−10293.

(6) Akhmetshina, A. I.; Ignat'eva, E. K.; Deberdeev, T. R.; Karimova, L. K.; Yuminova, Y. N.; Berlin, A. A.; Deberdeev, R. Y. Thermotropic liquid crystalline polyesters with mesogenic fragments based on the *p*-oxybenzoate unit. *Polym. Sci., Ser. D* **2019**, *12*, 427−434.

(7) Han, H.; Bhowmik, P. K. Wholly aromatic liquid-crystalline polyesters. *Prog. Polym. Sci.* **1997**, *22*, 1431−1502.

(8) Wei, P.; Lou, H.; Yan, J.; Li, L.; Zhang, Y.; Xia, Y.; Wang, Y.; Wang, Y. Synthesis and properties of high performance aromatic thermotropic liquid crystal copolyesters base on naphthalene ring structure. *Polymer* **2022**, *240*, No. 124472.

(9) Bhowmik, P. K.; Han, H.; Cebe, J. J.; Burchett, R. A. Thermotropic liquid-crystalline polyesters of 4,4′-biphenol and phenyl substituted 4,4′-biphenols with 4,4′-oxybisbenzoic acid. *J. Polym. Sci., Part A: Polym. Chem.* **2002**, *40*, 141−155.

(10) Sinta, R.; Gaudiana, R. A.; Minns, R. A.; Rogers, H. G. Para-linked, aromatic, thermotropic polyesters with low mesophase temperatures. *Macromolecules* **1987**, *20*, 2374−2382.

(11) Singh, M.; Takada, K.; Kaneko, T. Biobased liquid crystalline poly(coumarate)s composites and their potential applications. *Compos. Commun.* **2020**, *22*, No. 100531.

(12) Kneko, T.; Thi, T. H.; Shi, D. J.; Akashi, M. Environmentally degradable, high-performance thermoplascitcs from phenolic phyto-monomers. *Nat. Mater.* **2006**, *5*, 966−970.

(13) Cai, R.; Samulski, E. T. Liquid-crystalline aromatic polyesters containing isophthalic acid. *Macromolecules* **1994**, *27*, 135−140.

(14) Bhowmik, P. K.; Han, H. Fully aromatic liquid-crystalline polyesters of phenyl-substituted 4,4′-biphenols and 1,1′-binaphthyl-4,4′-diol with either 2-bromoterephthalic acid or 2-phenylterephthalic acid. *Macromolecules* **1993**, *26*, 5287−5294.

(15) Chang, S.; Han, C. D. Effect of flexible spacer length on the phase transitions and mesophase structures of main-chain thermo-

tropic liquid crystalline polyesters having bulky pendant side groups. *Macromolecules* **1997**, *30*, 1670−1684.
(16) Lenz, R. W. Synthesis and properties of thermotropic liquid crystal polymers with main chain mesogenic units. *Polym. J.* **1985**, *17*, 105−115.
(17) Ogawa, Y.; Ootani, K. Phase transitions of dimeric liquid crystals containing long odd-numbered methylene spacers. *Polym. J.* **1999**, *31*, 51−54.
(18) Martínez-Gómez, A.; Encinar, M.; Fernández-Blázquez, J. P.; Rubio, R. G.; Pérez, E. Relationship Between Composition, Structure and Dynamics of Main-Chain Liquid Crystalline Polymers with Biphenyl Mesogens. In *Liquid Crystalline Polymers*; Springer: Cham, 2015; pp 453−476 DOI: 10.1007/978-3-319-22894-5_15.
(19) Mather, P. T.; Romo-Uribe, A.; Han, C. D.; Kim, S. S. Rheo-optical evidence of a flow-induced isotropic-nematic transition in a thermotropic liquid-crystalline polymer. *Macromolecules* **1997**, *30*, 7977−7989.
(20) Watanabe, J.; Hayashi, M. Thermotropic liquid crystals of polyesters having a mesogenic p,p′-bibenzoate unit. 1. Smectic A mesophase properties of polyesters composed of p,p′-bibenzoic acid and alkylene glycols. *Macromolecules* **1988**, *21*, 278−280.
(21) Watanabe, J.; Hayashi, M. Thermotropic liquid crystals of polyesters having a mesogenic p,p′-bibenzoate unit. 2. X-ray study on smectic mesophase structures of BB-5 and BB-6. *Macromolecules* **1989**, *22*, 4083−4088.
(22) Tokita, M.; Osada, K.; Watanabe, J. Thermotropic Liquid Crystals of Main-chain Polyesters Having a Mesogenic 4,4′-Biphenyldicarboxylate Unit XI. Smectic Liquid Crystalline Glass. *Polym. J.* **1998**, *30*, 589−595.
(23) Ishige, R.; Tokita, M.; Funaoka, S.; Kang, S.; Watanae, J. Two-Step Smectic CA Phase Formation from Isotropic Liquid upon Supercooling in Main-Chain Liquid-Crystalline BB-5(1-Me) Polyester. *Macromol. Chem. Phys.* **2011**, *212*, 48−54.
(24) Osada, K.; Koike, M.; Tagawa, H.; Tokita, M.; Watanabe, J. Thermotropic Liquid Crystals of Main-Chain Polyesters having a Mesogenic 4,4′-Biphenyldicarboxylate Unit, 14. *Macromol. Chem. Phys.* **2004**, *205*, 1051−1057.
(25) Uchimura, M.; Ishige, R.; Shigeta, M.; Arakawa, Y.; Niko, Y.; Watanabe, J.; Konishi, G. Synthesis and properties of thermotropic liquid-crystalline polyesters containing 9,10-diphenylanthracence moiety in the main chain. *Res. Chem. Intermed.* **2013**, *39*, 403−414.
(26) Muthukumar, M.; Ober, C. K.; Thomas, E. L. Competing Interactions and Levels of Ordering in Self-Organizing Polymeric Materials. *Science* **1997**, *277*, 1225−1232.
(27) Hamley, I. W.; Castelletto, V.; Lu, Z. B.; Imrie, T.; Itoh, T.; Al-Hussein, M. Interplay between Smectic Ordering and Microphase Separation in a Series of Side-Group Liquid-Crystal Block Copolymers. *Macromolecules* **2004**, *37*, 4798−4807.
(28) Osuji, C.; Ferreira, P. J.; Mao, G.; Ober, C. K.; Sande, J. B. V.; Thomas, E. L. Alignment of Self-Assembled Hierarchical Microstructure in Liquid Crystalline Diblock Copolymers Using High Magnetic Fields. *Macromolecules* **2004**, *37*, 9903−9908.
(29) Tokita, M.; Adachi, M.; Masuyama, S.; Takazawa, F.; Watanabe, J. Characteristic Shear-Flow Orientation in LC Block Copolymer Resulting from Compromise between Orientations of Microcylinder and LC Mesogen. *Macromolecules* **2007**, *40*, 7276−7282.
(30) Iino, H.; Hanna, J. Liquid Crystalline Organic Semiconductors for Organic Transistor Applications. *Polym. J.* **2017**, *49*, 23−30.
(31) Brehmer, M.; Brömmel, F.; Cordoyiannis, G.; Jeu, W. H.; de Finkelmann, H.; Kramer, D.; Kutnjak, Z.; Lebar, A.; Ohm, C.; Ostrovskii, B. I.; Palffy-Muhoray, P.; Urayama, K.; Zalar, B.; Zentel, R. *Liquid Crystal Elastomers: Materials and Applications*; Springer Press, 2012.
(32) Hird, M. Fluorinated liquid crystals-properties and applications. *Chem. Soc. Rev.* **2007**, *36*, 2070−2095.
(33) Gray, G. W.; Hird, M.; Ifill, A. D.; Smith, W. E.; Toyne, K. J. The synthesis and transition temperatures of some 4′-alkyl- and 4′-alkoxy-4-cyano-3-fluorobiphenyls. *Liq. Cryst.* **1995**, *19*, 77−83.
(34) Antoun, S.; Lenz, R. W.; Jin, J. -I. Liquid crystal polymers. IV. Thermotropic polyesters with flexible spacers in the main chain. *J. Polym. Sci. Polym. Chem. Ed.* **1981**, *19*, 1901−1920.
(35) Mather, P.; Grizzuti, N.; Heffner, G.; Ricker, M.; Rochefort, W. E.; Seitz, M.; Schmidt, H-W.; Pearson, D. S. Synthesis and characterization of a semiflexible liquid crystalline polyester with a broad nematic region. *Liq. Cryst.* **1994**, *17*, 811−826.
(36) Ober, C. K.; Jin, J. I.; Zhou, Q.; Lenz, R. W. Liquid crystal polymers with flexible spacers in the main chain. In *Liquid Crystal Polymers I. Advances in Polymer Science*; Springer: Berlin, Heidelbelg press1984; Vol. *59* DOI: 10.1007/3-540-12818-2_8.
(37) Gray, G. W.; Jones, B.; Marson, F. 71. Mesomorphism and chemical constitution. Part VIII. The effect of 3′-substituents on the mesomorphism of the 4′-*n*-alkoxydipheynl-4-carboxylic acids and their alkyl esters. *J. Chem. Soc.* **1957**, 393−401.
(38) Nakata, Y.; Hayashi, M.; Tokita, M.; Osada, K.; Watanabe, J. Smectic characteristics of main-chain polyesters as elucidated from a variation of layer thickness with carbon number of aliphatic spacer in a wide range, 5 to 20. *High Perform. Polym.* **1998**, *10*, 121−130.
(39) Arakawa, Y.; Kang, S.; Tsuji, H.; Watanabe, J.; Konishi, G. The design of liquid crystalline bistolane-based materials with extremely high birefringence. *RSC Adv.* **2016**, *6*, 92845−92851.
(40) Arakawa, Y.; Kang, S.; Tsuji, H.; Watanabe, J.; Konishi, G. Development of novel bistolane-based liquid crystalline molecules with an alkylsulfanyl group for highly birefringent materials. *RSC Adv.* **2016**, *6*, 16568−16574.
(41) Lou, S.; Fu, G. C. Palladium/Tris(*tert*-butyl)phosphine-Catalyzed Suzuki Cross-Couplings in the presence of Water. *Adv. Synth. Catal.* **2010**, *352*, 2081−2084.
(42) Yu, X.; Wang, Z.; Buchhols, M.; Füllgrabe, N.; Grosjean, S.; Bebensee, F.; Bräse, S.; Wöll, C.; Heinke, L. *cis*-to-*trans* isomerization of azobenzene investigated by using thin films of metal-organic frameworks. *Phys. Chem. Chem. Phys.* **2015**, *17*, 22721−22725.
(43) McMillan, W. L. Simple Molecular Model for the Smectic *A* phase of Liquid Crystals. *Phys. Rev. A* **1971**, *4*, 1238−1246.
(44) Cohen, S. D.; Diugiuid, C. A. D.; Poirier, J. C.; Swadesh, J. K. Synthesis and Thermal Analysis of Fourteen Homologous Mesogenic Monoesters of Biphenyl-4,4′-dicarboxylic Acid. *Mol. Cryst. Liq. Cryst.* **1981**, *78*, 135−155.
(45) Laus, M.; Angeloni, A. S.; Galli, G.; Chiellini, E. Molecular weight and molecular weight distribution effects on the liquid-crystalline and biphasic behavior of a thermotropic polyester. *Macromolecules* **1992**, *25*, 5901−5906.
(46) Sarasua, J-R.; Prud'homme, R. E.; Wisniewski, M.; Le Borgne, A.; Spassky, N. Crystallization and Melting Behavior of Polyactides. *Macromolecules* **1998**, *31*, 3895−3905.
(47) Frisch, M. J.; Trucks, G. W.; Schlegel, H. B.; Scuseria, G. E.; Robb, M. A.; Cheeseman, J. R.; Scalmani, G.; Barone, V.; Mennucci, B.; Petersson, G. A.; Nakatsuji, H.; Caricato, M.; Li, X.; Hratchian, H. P.; Izmaylov, A. F.; Bloino, J.; Zheng, G.; Sonnenberg, J. L.; Hada, M.; Ehara, M.; Toyota, K.; Fukuda, R.; Hasegawa, J.; Ishida, M.; Nakajima, T.; Honda, Y.; Kitao, O.; Nakai, H.; Vreven, T.; Montgomery, J. A., Jr.; Peralta, J. E.; Ogliaro, F.; Bearpark, M.; Heyd, J. J.; Brothers, E.; Kudin, K. N.; Staroverov, V. N.; Keith, T.; Kobayashi, R.; Normand, J.; Raghavachari, K.; Rendell, A.; Burant, J. C.; Iyengar, S. S.; Tomasi, J.; Cossi, M.; Rega, N.; Millam, J. M.; Klene, M.; Knox, J. E.; Cross, J. B.; Bakken, V.; Adamo, C.; Jaramillo, J.; Gomperts, R.; Stratmann, R. E.; Yazyev, O.; Austin, A. J.; Cammi, R.; Pomelli, C.; Ochterski, J. W.; Martin, R. L.; Morokuma, K.; Zakrzewski, V. G.; Voth, G. A.; Salvador, P.; Dannenberg, J. J.; Dapprich, S.; Daniels, A. D.; Farkas, O.; Foresman, J. B.; Ortiz, J. V.; Cioslowski, J.; Fox, D. J. *Gaussian 09*, Revision D.01; Gaussian, Inc.: Wallingford CT, 2013.
(48) Arai, T.; Biely, P.; Uhliariková, I.; Sato, N.; Makishima, S.; Mizuno, M.; Nozaki, K.; Kaneko, S.; Amano, Y. Structural characterization of hemicellulose released from corn cob in continuous flow type hydrothermal reactor. *J. Biosci. Bioeng.* **2019**, *127*, 222−230.


https://doi.org/10.1021/acs.macromol.3c00773
*Macromolecules* 2023, 56, 5152−5161

(49) Issam, A. M.; Hena, S.; Khizrien, A. K. N. A New Unsaturated Poly(ester-urethane) Based on Terephthalic Acid Derived from Polyethylene Terephthalate (PET) of Waste Bottles. *J. Polym. Environ.* **2012**, *20*, 469−476.
(50) Yamazaki, S.; Tokita, M. A Correlation between Thermal Diffusivity and Long Period in Thermotropic Liquid Crystalline Polyesters. *Macromolecules* **2019**, *52*, 9781−9785.
(51) Arakawa, Y.; Nakajima, S.; Kang, S.; Konishi, G.; Watanabe, J. Synthesis and evaluation of high-birefringence polymethacrylate having a diphenyl-diacetylene LC moiety in the side chain. *J. Mater. Chem.* **2012**, *22*, 14346−14348.
(52) Kang, S.; Nakajima, S.; Arakawa, Y.; Tokita, M.; Watanabe, J.; Konishi, G. Highly birefringent side-chain LC polymethacrylate with a dinaphthyl-acetylene mesogenic unit. *Polym. Chem.* **2014**, *5*, 2253−2258.
(53) Picken, S. J.; Sikkema, D. J.; Boerstoel, H.; Dingemans, T. J.; van der Zwaag, S. Liquid crystal main-chain polymers for high-performance fibre applications. *Liq. Cryst.* **2011**, *38*, 1591−1605.



https://doi.org/10.1021/acs.macromol.3c00773
*Macromolecules* 2023, 56, 5152−5161